Load and Mutual Inductance Identification From the Primary Side of Inductive Power Transfer System With Parallel-Tuned Secondary Power Pickup

Yu-Gang Su, *Member, IEEE*, Long Chen, Xue-Ying Wu, Aiguo Patrick Hu, *Senior Member, IEEE*, Chun-Sen Tang, *Member, IEEE*, and Xin Dai, *Member, IEEE*

***Abstract*—An important feature of an inductive power transfer (IPT) system is its power transfer efficiency and capability can be significantly affected by the load and the magnetic coupling variations. Therefore, identifying the load and the mutual inductance is essential to improve the system performance. This paper proposes a load and mutual inductance identification method for IPT systems with parallel-compensated power pickups based only on the information detected from the primary side. The proposed method can be implemented for primary resonant circuits whether they are series or parallel tuned, or with a hybrid compensation, such as an LCL configuration. An identification model is established according to the steady-state characteristics of the system. Identification results are obtained based on mathematical derivations and analyses. The proposed identification method is realized without any extra communication or control, and both the simulation and experimental results have verified its feasibility.**

***Index Terms*—Inductive power transfer (IPT), load identification, mutual inductance identification, wireless power transfer (WPT).**

I. Introduction

As ONE of wireless power transfer (WPT) technologies, inductive power transfer (IPT) technology has attracted a wide attention recently [1]–[3]. It has become a crucial technology in various fields, such as transportation applications [4]–[6], lighting applications [7], [8], electronic products [9], [10], and biomedical implants [11], [12] due to its safety, reliability, and flexibility. In recent years, lots of research efforts have been devoted to improve the transfer efficiency and the capability of IPT systems, both of which are significantly affected by the load and the strength of the magnetic coupling [13]–[15]. In some applications, the variations of the load and the mutual inductance are inevitable and cannot be neglected. Taking the wireless power supply for electric vehicles (EVs) as an example, different EVs have the different power requirements as well as the load characteristics, and the different mutual inductances because of the different vertical heights and the alignment of chassis which may change the air gap between the transmitting winding and the pick-up winding. A wireless communication system is often used to set up on the secondary side to provide the feedback signals to the primary [16]–[18]. However, removing the additional communication system between the primary side and the secondary side will obviously decrease the system volume, cost, and complexity.

Currently, a certain achievements in the load identification of IPT system when the mutual inductance is invariable have gained by a number of scholars [19]–[22]. Literature [23] achieves the load and the mutual inductance identification of the S/S-type IPT system based on an additional compensating capacitor in the primary side. However, this method increases the complexity of the system and the control difficulty. In [24], the mutual inductance and load resistance of WPT system was identified when the operating frequency is different from resonant frequency of the receiver. Similarly, this method is focused only on the S/S-type IPT system. There is almost no research being reported for identifying the load and the mutual inductance of secondary parallel-compensated IPT systems which are widely used in practice due to its voltage boosting property and inherent current limiting capability [8], [13], [25], [26]. Although it is reported that two likely sets of identification solutions of a S/P-type IPT system will be derived based on the sampled input impedance at any operating frequency in [24], there is no study to eliminate the undesired solution of the two sets of identification solutions. In addition, it is also found that two sets of identification solutions can be obtained for the P/P- and LCL/P-type IPT systems in the paper. The method to obtain the actual identification results from the two sets has not been reported.

This paper proposes a method of identifying load and mutual inductance of the secondary parallel-compensated IPT

Manuscript received September 11, 2017; revised November 25, 2017; accepted January 5, 2018. Date of publication January 15, 2018; date of current version August 7, 2018. This work was supported by research funds from the National Natural Science Foundation of China under Grant 51477020 and Grant 61573074. Recommended for publication by Associate Editor R. Hui. *(Corresponding author: Yu-Gang Su.)*

Y.-G. Su is with the Key Laboratory of Dependable Service Computing in Cyber Physical Society, Chongqing University, Ministry of Education, Chongqing 400044, China and also with the College of Automation, Chongqing University, Chongqing 400044, China (e-mail: su7558@qq.com).

L. Chen, X.-Y. Wu, C.-S. Tang, and X. Dai are with the College of Automation, Chongqing University, Chongqing 400044, China (e-mail: 365852249@qq.com; 975623914@qq.com; cstang@cqu.edu.cn; toybear@vip.sina.com).

A. P. Hu is with the Department of Electrical and Computer Engineering, University of Auckland, Auckland 1142, New Zealand (e-mail: a.hu@auckland.ac.nz).

Color versions of one or more of the figures in this paper are available online at http://ieeexplore.ieee.org.

Digital Object Identifier 10.1109/TPEL.2018.2793854

See http://www.ieee.org/publications_standards/publications/rights/index.html for more information.

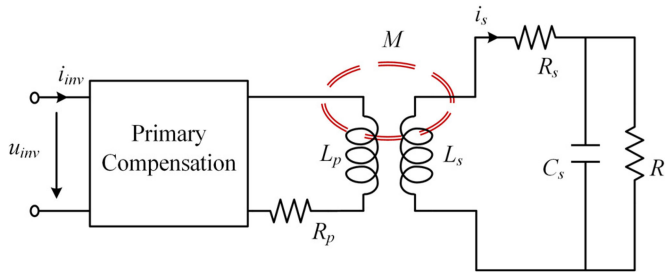

Fig. 1. Equivalent circuit of the secondary parallel-compensated IPT system.

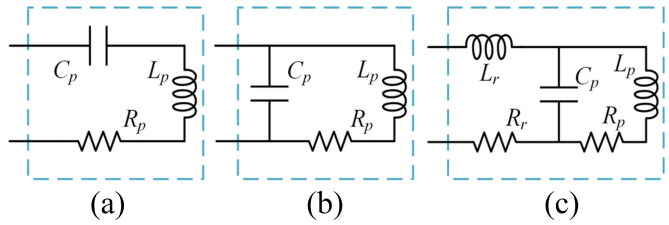

Fig. 2. (a) Series, (b) parallel, and (c) LCL compensation in the primary side.

systems. The method can be implemented regardless of the compensation topologies of the primary resonant circuit, which can be either series, parallel, or hybrid compensations, such as LCL. The process to eliminate the undesired solution is described in details. Only the information of the system operating frequency, the output voltage, and current of the primary power inverter are required for load and mutual inductance by this method. Furthermore, this identification method can be achieved without any extra communication or control circuits, therefore, the cost and complexity of the system is kept low.

This paper is organized as follows. Section II introduces the three basic circuit topologies of secondary parallel-compensated IPT systems. Then, the proposed identification model is built and the corresponding analyses are conducted in Section III. Section IV provides the simulations and the experiments. Finally, Section V concludes the whole paper.

II. System Overview

A. Circuit Topology

The equivalent circuit topology of the secondary parallel-compensated IPT systems is shown in Fig. 1.

The primary compensation module can be divided into three classes of the compensation schemes that are shown in Fig. 2. From Fig. 2(a) and (b), the primary coil L_p in series or parallel with the compensating capacitor C_p can constitute a series or parallel resonant tank. Besides, the LCL primary resonant tank is made up of the primary coil L_p in parallel with the compensating capacitor C_p and the series inductor L_r shown in Fig. 2(c). In the secondary side, the secondary coil receives power from the high-frequency magnetic field and the parallel resonant network which is composed of the resonant inductor L_s and the parallel capacitor C_s. The equivalent load R picks up the power from the secondary side via the resonant network. R_p, R_s and R_r are the inherent resistances of the primary coil L_p, the secondary coil L_s and the series inductor L_r, respectively. M is the mutual inductance between the primary and secondary coils. $u_{\rm inv}$ and $i_{\rm inv}$ are the output voltage and current of inverter, respectively.

TABLE I
RMS Values of Output Voltage and Current of Inverter

	Series compensation	Parallel compensation	LCL compensation
$U_{\rm inv}$	$U_{\rm mea}$	$U_{\rm mea}$	$\frac{4}{\sqrt{2}\pi} U_{\rm mea}$
$I_{\rm inv}$	$I_{\rm mea}$	$\frac{4}{\sqrt{2}\pi} I_{\rm mea}$	$I_{\rm mea}$

B. Nominal Resonant Frequency

In order to minimize the volt-ampere (VA) rating of the power supply and achieve the maximum power transfer capability, it is a logical choice to design the primary and secondary nominal resonant frequency at or near a same frequency ω_0. Therefore, the circuit parameters designed in this paper satisfy the following relationship:

$$\omega_0^2 \approx \begin{cases} \dfrac{1}{L_p C_p} \approx \dfrac{1}{L_s C_s} & \text{S/P \& P/P} \\ \dfrac{1}{C_p L_r L_p / (L_r + L_p)} \approx \dfrac{1}{L_s C_s} & \text{LCL/P} \end{cases}. \quad (1)$$

C. Output Voltage and Current of Inverter

In the primary side, the inductor and the capacitor serve as a low-pass filter and the high frequency harmonic currents in the resonant network are suppressed. Therefore, only the fundamental harmonic is considered for power transfer based on the Fourier decomposition. Then, the root-mean-square (RMS) values of $u_{\rm inv}$ and $i_{\rm inv}$ can be calculated as shown in Table I. $U_{\rm mea}$ and $I_{\rm mea}$ represent the measured RMS values of the output voltage and current of the inverter, respectively.

III. Load and Mutual Inductance Identification Method

Before the theoretical analysis, there are some assumptions that need to be made:

1) the circuit parameters, namely L_p, L_s, L_r, C_p, C_s, R_p, R_s, R_r, are measured and known;
2) under normal circuit operating conditions, these circuit parameters do not change much, therefore, they are considered to be constant [19]–[24].

A. Circuit Model

From Fig. 1, the Kirchhoff voltage law equation can be derived as

$$\begin{bmatrix} \dot{I}_{\rm inv} \\ \dot{I}_s \end{bmatrix} = \begin{bmatrix} Z_{11} & Z_{12} \\ Z_{21} & Z_{22} \end{bmatrix}^{-1} \cdot \begin{bmatrix} \dot{U}_{\rm inv} \\ 0 \end{bmatrix}. \quad (2)$$

The expressions of Z_{11}, Z_{12}, Z_{21}, and Z_{22} for the primary-resonant tank are listed in Table II. ω is the angular frequency

TABLE II
EXPRESSIONS OF Z_{11}, Z_{12}, Z_{21}, AND Z_{22}

	S/P	P/P	LCL/P
Z_{11}	$R_p + j\cdot(\omega L_p - \frac{1}{\omega C_p})$	$\frac{j\omega L_p + R_p}{\varphi}$	$j\omega L_r + R_r + \frac{j\omega L_p + R_p}{\varphi}$
$Z_{12} = Z_{21}$	$j\gamma$	$\frac{j\gamma}{\varphi}$	$\frac{j\gamma}{\varphi}$
Z_{22}	Z_s	$Z_s - \frac{j\omega C_p \gamma^2}{\varphi}$	$Z_s - \frac{j\omega C_p \gamma^2}{\varphi}$

in the system, where

$$\varphi = \alpha_1 + j\cdot\beta_1 = \left(1 - \omega^2 L_p C_p\right) + j\omega C_p R_p \tag{3}$$

$$\gamma = \omega M. \tag{4}$$

For the convenience of derivation, the variable $\psi = \omega C_s R$ is defined and then the impedance of the secondary network Z_s is expressed as

$$\begin{aligned} Z_s &= \alpha_2 + j\cdot\beta_2 \\ &= R_s + \frac{\psi}{\omega C_s\left(1+\psi^2\right)} + j\left[\omega L_s - \frac{\psi^2}{\omega C_s\left(1+\psi^2\right)}\right]. \end{aligned} \tag{5}$$

Based on (2), the expression of $\dot{I}_{\text{inv}}$ is conducted

$$\dot{I}_{\text{inv}} = \frac{\begin{vmatrix} \dot{U}_{\text{inv}} & Z_{12} \\ 0 & Z_{22} \end{vmatrix}}{\begin{vmatrix} Z_{11} & Z_{12} \\ Z_{21} & Z_{22} \end{vmatrix}}. \tag{6}$$

Then, the input impedance Z_{in} can be derived from (6)

$$Z_{\text{in}} = \frac{\dot{U}_{\text{inv}}}{\dot{I}_{\text{inv}}} = Z_{11} - \frac{Z_{12}^2}{Z_{22}}. \tag{7}$$

Generally, in order to minimize the VA ratings of the power supply, it is desirable to make the IPT systems operate at zero phase angle (ZPA) frequency [6], [27]. At this frequency, u_{inv} and i_{inv} should be in phase and the following relationships are obtained

$$\Re\left(Z_{\text{in}}\right) = \frac{U_{\text{inv}}}{I_{\text{inv}}} \tag{8}$$

$$\Im\left(Z_{\text{in}}\right) = 0 \tag{9}$$

where $\Re$ and $\Im$ represent the real and imaginary component of the corresponding variable, respectively. Further, the following equation is conducted based on (7)

$$\frac{1}{Z_{11} - \frac{U_{\text{inv}}}{I_{\text{inv}}}} = \frac{Z_{22}}{Z_{12}^2}. \tag{10}$$

Defining

$$Z_\theta = \frac{1}{Z_{11} - \frac{U_{\text{inv}}}{I_{\text{inv}}}}. \tag{11}$$

Then, (10) can be expressed as follows:

$$\Re\left(Z_\theta\right) = \Re\left(\frac{Z_{22}}{Z_{12}^2}\right) \tag{12}$$

$$\Im\left(Z_\theta\right) = \Im\left(\frac{Z_{22}}{Z_{12}^2}\right). \tag{13}$$

B. Load and Mutual Inductance Identification

According to Table II, the value of Z_θ can be calculated, while the real and imaginary components of $\frac{Z_{22}}{Z_{12}^2}$ can be expressed. For the primary-series compensation

$$\begin{cases} \Re\left(\frac{Z_{22}}{Z_{12}^2}\right)_{-S} = -\frac{\alpha_2}{\gamma^2} \\ \Im\left(\frac{Z_{22}}{Z_{12}^2}\right)_{-S} = -\frac{\beta_2}{\gamma^2} \end{cases}. \tag{14}$$

For the primary-parallel and -LCL compensation

$$\begin{cases} \Re\left(\frac{Z_{22}}{Z_{12}^2}\right)_{-\text{P/LCL}} = \frac{\left(\beta_1^2 - \alpha_1^2\right)}{\gamma^2}\alpha_2 + \frac{2\alpha_1\beta_1}{\gamma^2}\beta_2 + \beta_1\omega C_p \\ \Im\left(\frac{Z_{22}}{Z_{12}^2}\right)_{-\text{P/LCL}} = \frac{\left(\beta_1^2 - \alpha_1^2\right)}{\gamma^2}\beta_2 - \frac{2\alpha_1\beta_1}{\gamma^2}\alpha_2 - \alpha_1\omega C_p \end{cases}. \tag{15}$$

The subscript $-S$ indicates that the parameter is for series-compensated primary circuit, and –P/LCL is used to indicate the parallel and LCL compensation. Such a notation will be used for other variables throughout this paper.

From (4) and (5), it can be seen that the mutual inductance *M* is only included in γ, while the equivalent resistance *R* is included in α_2 and β_2. Therefore, all the variables in (14) and (15) are known previously except α_2, β_2 and γ. By substituting (12) and (13) into (14) and (15), respectively, the variable γ can be eliminated and a general equation related to the variable ψ is obtained

$$m_1\psi^2 + m_2\psi + m_3 = 0. \tag{16}$$

For the primary-series compensation

$$\begin{cases} m_1 = \Re\left(Z_\theta\right)\cdot\left(\omega^2 C_s L_s - 1\right) - \Im\left(Z_\theta\right)\cdot\omega C_s R_s \\ m_2 = -\Im\left(Z_\theta\right) \\ m_3 = \omega C_s\left[\Re\left(Z_\theta\right)\cdot\omega L_s - \Im\left(Z_\theta\right)\cdot R_s\right] \end{cases}. \tag{17}$$

For the primary-parallel and -LCL compensation

$$\begin{cases} m_1 = \omega^2 L_s C_s \left(k_2 k_4 - k_1 k_3\right) + \omega C_s R_s \left(k_1 k_4 + k_2 k_3\right) \\ \qquad +k_1 k_3 - k_2 k_4 \\ m_2 = k_1 k_4 + k_2 k_3 \\ m_3 = \omega^2 L_s C_s \left(k_2 k_4 - k_1 k_3\right) + \omega C_s R_s \left(k_1 k_4 + k_2 k_3\right) \end{cases} \tag{18}$$

where

$$\begin{cases} k_1 = \beta_1^2 - \alpha_1^2 \\ k_2 = 2\alpha_1\beta_1 \\ k_3 = \Re\left(Z_\theta\right) - \beta_1 \omega C_p \\ k_4 = \Im\left(Z_\theta\right) + \alpha_1 \omega C_p \end{cases}. \tag{19}$$

Finally, deriving from (16), ψ can be calculated easily

$$\begin{cases} \psi_1 = \frac{-m_2 + \sqrt{m_2^2 - 4m_1 m_3}}{2m_1} \\ \psi_2 = \frac{-m_2 - \sqrt{m_2^2 - 4m_1 m_3}}{2m_1} \end{cases}. \tag{20}$$

Then, two group expressions of R and M can be calculated based on ψ_1 and ψ_2. For the primary-series compensation

$$\begin{cases} R_i = \frac{\psi_i}{\omega C_s} \\ M_i = \frac{1}{\omega}\sqrt{-\frac{\omega C_s R_s\left(1+\psi_i^2\right)+\psi_i}{\omega C_s\left(1+\psi_i^2\right)\Re(Z_\theta)}} \end{cases}, \quad i = 1, 2. \tag{21}$$

For the primary-parallel and LCL compensation (22) shown at the bottom of this page.

From (20) to (22), it can be seen that there are two solutions of ψ that lead to two sets of calculated results. Obviously, one set of the calculated results is the actual identification result, and the other set would be an undesired solution which should be eliminated.

In order to obtain the actual identification results, the sign of ψ_1 and ψ_2 should be analysed first. Because at least one solution of ψ is positive, there are following two remaining cases:

1) either of them is positive (i.e., $\psi_1\psi_2 < 0$);

2) both of them are positive (i.e., $\psi_1\psi_2 > 0$).

Taking the S/P type as an example, the normalized angular frequency $\omega_n = \omega/\omega_0$ is defined and then the parameters Z_θ, m_1, and m_3 are rewritten as follows:

$$\begin{cases} Z_\theta = \dfrac{\left(R_p - K\right) + j\varpi\omega_0 L_p}{\left(R_p - K\right)^2 + \varpi^2\omega_0^2 L_p^2} \\ m_1 = -\omega_n\left[\varpi \cdot \Re\left(Z_\theta\right) + \omega_0 C_s R_s \cdot \Im\left(Z_\theta\right)\right] \\ m_3 = \omega_n\left[\omega_n \cdot \Re\left(Z_\theta\right) - \omega_0 C_s R_s \cdot \Im\left(Z_\theta\right)\right] \end{cases} \tag{23}$$

where

$$\begin{cases} \varpi = \frac{1}{\omega_n} - \omega_n \\ K = \frac{U_{\text{inv}}}{I_{\text{inv}}} \end{cases}. \tag{24}$$

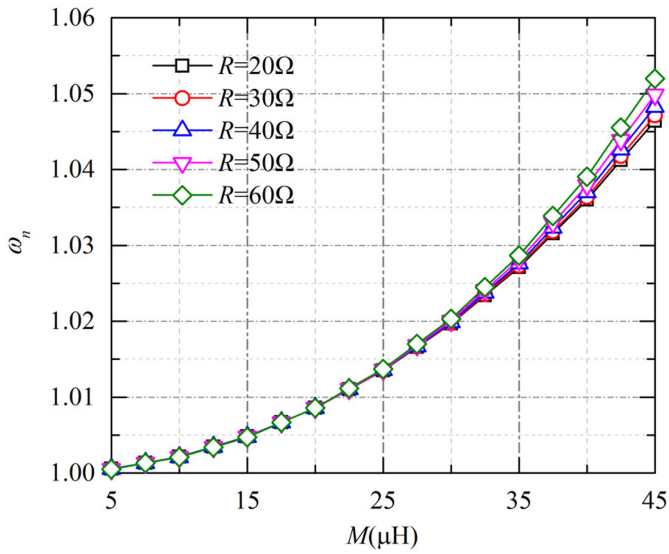

Fig. 3. Normalized angular frequency (ω_n) of primary series compensation versus M at different R.

From (16), it can be seen that $\psi_1\psi_2$ and $m_1 m_3$ have the same sign according to the Vieta's formulas.

$$\psi_1\ \psi_2 = \frac{m_3}{m_1}. \tag{25}$$

It is found that the values of m_1 and m_3 are determined by ω_n from (23). When the load and the mutual inductance vary, the system operating frequency will be changed to achieve the ZPA condition. According to (7) and Table II, (9) can be regarded as an equation related to R, M and ω, which is expressed as

$$\Im\left(Z_{11} - \frac{Z_{12}^2}{Z_{22}}\right) = f\left(R, M, \omega\right) = 0. \tag{26}$$

Thus, the values of ω_n at different load resistances and mutual inductances can be calculated based on (26). The results are illustrated in Fig. 3.

From Fig. 3, it can be seen that M has a major influence on ω_n which increases with the growing M, and the minimum value of ω_n is about 1.005 when M is set at 5.00 μH (the coupling coefficient k is about 0.033). However, the coupling coefficient of IPT systems is typically in the range of 0.1–0.3 [28] (the mutual inductance of the three systems in this paper ranges from approximately 15 to 45 μH). Thus, ω_n is considered larger than 1 under the most ordinary operating condition.

The coupling coefficient k of IPT systems is defined as

$$k = \frac{M}{\sqrt{L_p L_s}}. \tag{27}$$

According to (26), M can be expressed by R and ω

$$M = g\left(R, \omega\right). \tag{28}$$

$$\begin{cases} R_i = \frac{\psi_i}{\omega C_s} \\ M_i = \frac{1}{\omega}\sqrt{\frac{\left(\beta_1^2-\alpha_1^2\right)\left[\omega R_s C_s\left(1+\psi_i^2\right)+\psi_i\right]+2\alpha_1\beta_1\left[\omega^2 L_s C_s\left(1+\psi_i^2\right)-\psi_i^2\right]}{\omega C_s\left(1+\psi_i^2\right)\left[\Re(Z_\theta)+\beta_1\omega C_p\right]}} \end{cases}, \quad i = 1, 2 \tag{22}$$

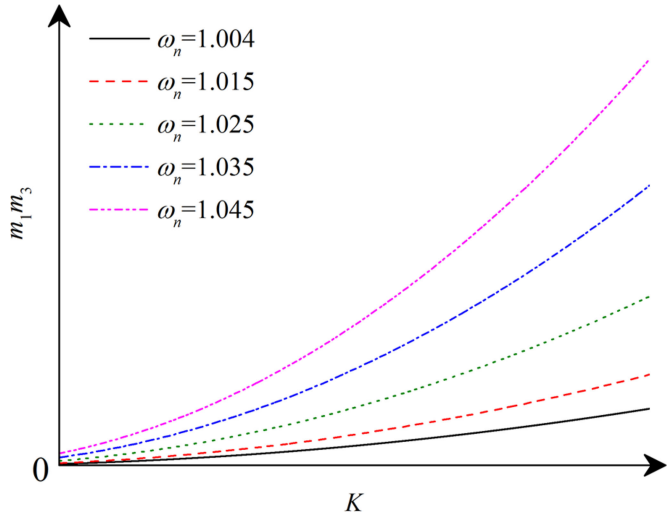

Fig. 4. Curves of $m_1 m_3$ at different ω_n when the primary-resonant tank is series compensation.

By substituting (28) into (27), the expression of k can be obtained

$$k = \frac{g(R,\omega)}{\sqrt{L_p L_s}}. \tag{29}$$

Further, (30) can be derived from (29) according to (3) and (5).

$$k = \sqrt{\frac{\alpha_1(\alpha_2^2+\beta_2^2)}{\omega_n\omega_0 L_s\beta_2(1-\alpha_1)}}. \tag{30}$$

Making

$$\frac{d}{dR}k = 0. \tag{31}$$

R_m corresponding to the maximum coupling coefficient can be obtained as

$$R_m = \frac{R_s}{\omega_n^2 - 1}. \tag{32}$$

When R approaches infinity, the minimum value of k can be achieved which is expressed in (33) together with the maximum value of k

$$\begin{cases} k_{\max} = k|_{R=R_m} = \sqrt{\frac{\omega_n^2+\lambda^2 R_s^2-1}{\omega_n^2}} \\ k_{\min} = k|_{R\to+\infty} = \sqrt{\frac{\omega_n^4+(\lambda^2 R_s^2-2)\omega_n^2+1}{\omega_n^4}} \end{cases}. \tag{33}$$

Then, the range of normalized angular frequency ω_n under general operating condition can be calculated by (34) and this range is about [1.005, 1.195]

$$\omega_n \in \{\omega_n > 1\} \cap \{k_{\max} \geq 0.1\} \cap \{k_{\min} \leq 0.3\}. \tag{34}$$

Under this condition, the curves of $m_1 m_3$ at different ω_n when the primary-resonant tank is series compensation are plotted in Fig. 4 based on (23).

Similarly, for the primary parallel- and LCL- compensated IPT systems, Fig. 5 shows the values of ω_n at different load resistances and mutual inductances. As the S/P type, ω_n of both

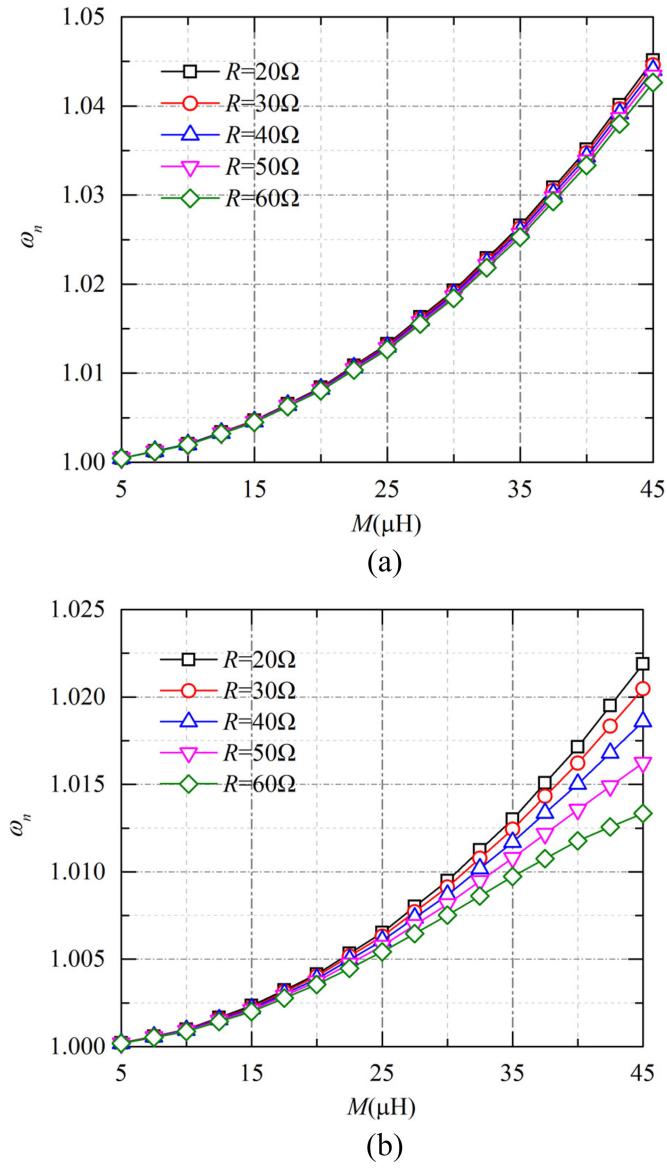

Fig. 5. Normalized angular frequency (ω_n) of primary (a) parallel and (b) LCL compensation versus M at different R.

the P/P and LCL/P type are larger than 1 when M is in the range of 15 to 45 μH.

Then, the ranges of normalized angular frequency ω_n under general operating condition can be calculated, and the curves of $m_1 m_3$ can be illustrated in Fig. 6.

For the primary LCL compensation, Fig. 6(b) shows that the values of $m_1 m_3$ are negative which means either ψ_1 or ψ_2 is positive. Further, it can be seen ψ_2 is positive from Fig. 7 and ψ_2 is considered as the solution that leads to the actual identification results.

On the other hand, for the primary series and parallel compensation, both ψ_1 and ψ_2 are positive according to Figs. 4 and 6(a). As discussed above, ψ_1 and ψ_2 are calculated based on the fundamental harmonic. Thus, in order to distinguish these two solutions, the RMS values of high order harmonics of i_{inv} are need to be calculated, and they can be calculated based on ψ_1

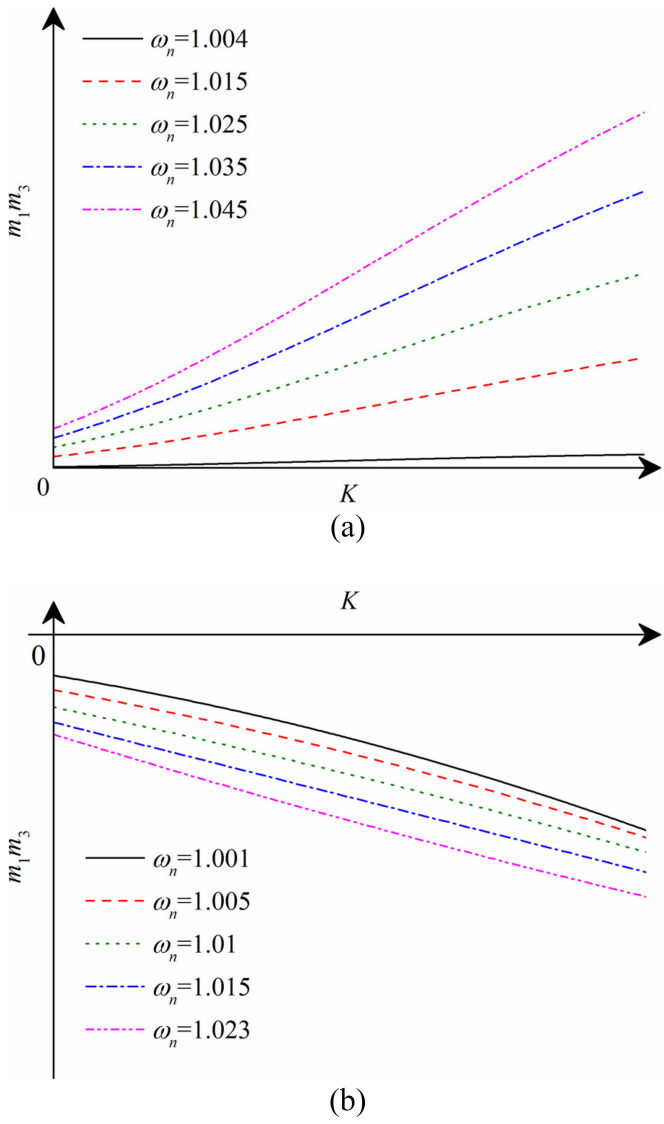

Fig. 6. Curves of $m_1 m_3$ at different ω_n when the primary-resonant tank is (a) parallel compensation and (b) LCL compensation.

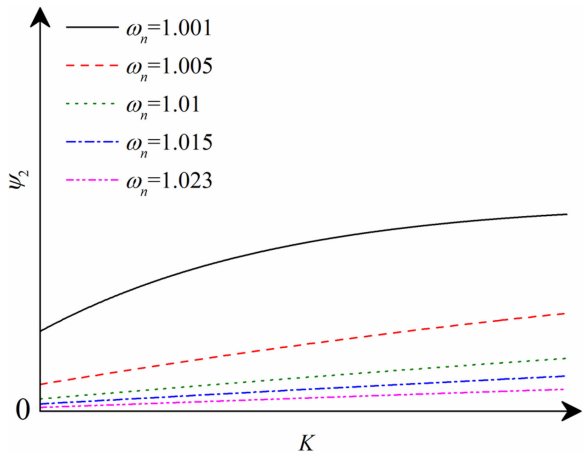

Fig. 7. Curves of ψ_2 at different ω_n when the primary-resonant tank is LCL compensation.

and ψ_2 respectively. Then, the two sets of calculated values are compared with the actual RMS values of high order harmonics of i_{inv}, and the solution which leads to the actual identification results can be obtained.

Still taking the S/P type as an example, the RMS values of i_{inv} for each harmonic order m are calculated as

$$I_{\text{inv}\ -i}^{(m)} = \frac{U_{\text{inv}}^{(m)}}{Z_{\text{in}}^{(m)}(R_i, M_i)}, \quad i = 1, 2; \quad m = 3, 5 \ldots 2k+1 \tag{35}$$

where R_i and M_i can be calculated based on ψ_i, respectively, by solving (21); $U_{\text{inv}}^{(m)}$ represents the RMS values of mth harmonic of u_{inv} and it can be calculated from

$$U_{\text{inv}}^{(m)} = \frac{4U_{\text{mea}}}{\sqrt{2}m\pi}. \tag{36}$$

Then, the mean-squared error between the measured values and the calculated values are computed

$$\sigma(n)_{-i} = \sqrt{\frac{\sum\limits_{m=3,5,\cdots,n} \varepsilon(m)_{-i}^2}{(n-1)/2}} \tag{37}$$

where

$$\varepsilon(m)_{-i} = I_{\text{inv}\ -\text{mea}}^{(m)} - I_{\text{inv}\ -i}^{(m)}. \tag{38}$$

Here, $I_{\text{inv\_mea}}^{(m)}$ represents the measured RMS values of the mth harmonic, and $\varepsilon(m)_{-i}$ can be calculated by combining (35). It is obvious that a smaller $\sigma(n)_{-i}$ means the values calculated based on ψ_i are closer to the measured values. Through the simulation analysis, it is found the identification results may be incorrect unless two or more harmonic components are taken into consideration. For instance, when R and M are set at 20.00 Ω and 35.00 μH, the identification results are 4255.40 Ω and 8.42 μH when only the third harmonic is taken into consideration, while the identification results are 20.34 Ω and 34.85 μH by considering the third and fifth harmonics. If more than two harmonic components are calculated in (37), it will make no difference to the identification results, but increase the computing cost. Thus, the RMS values of third and fifth harmonics are calculated in this paper, and μ is defined in (39) to find out the larger $\sigma(n)_{-i}$ which leads to the undesired solution

$$\mu = \sigma(5)_{-1} - \sigma(5)_{-2}. \tag{39}$$

Obviously, ψ_1 turns out to be the undesired solution when μ is positive, and the ψ_2 is considered as the undesired solution when a negative μ is achieved. For the primary parallel and LCL compensation, the undesired solution can be eliminated in the same method.

Finally, the identification results can be got by solving (21) or (22) depending on the compensation schemes of the primary-resonant tank. In conclusion, the identification procedure is described in Fig. 8.

In addition, ZPA frequency is selected as the operating frequency in many IPT systems to produce a unity power factor input [6], [27], thus the identification method is proposed for the systems which operate at ZPA frequency. However, this method can still be applied even if the system does not operate at ZPA

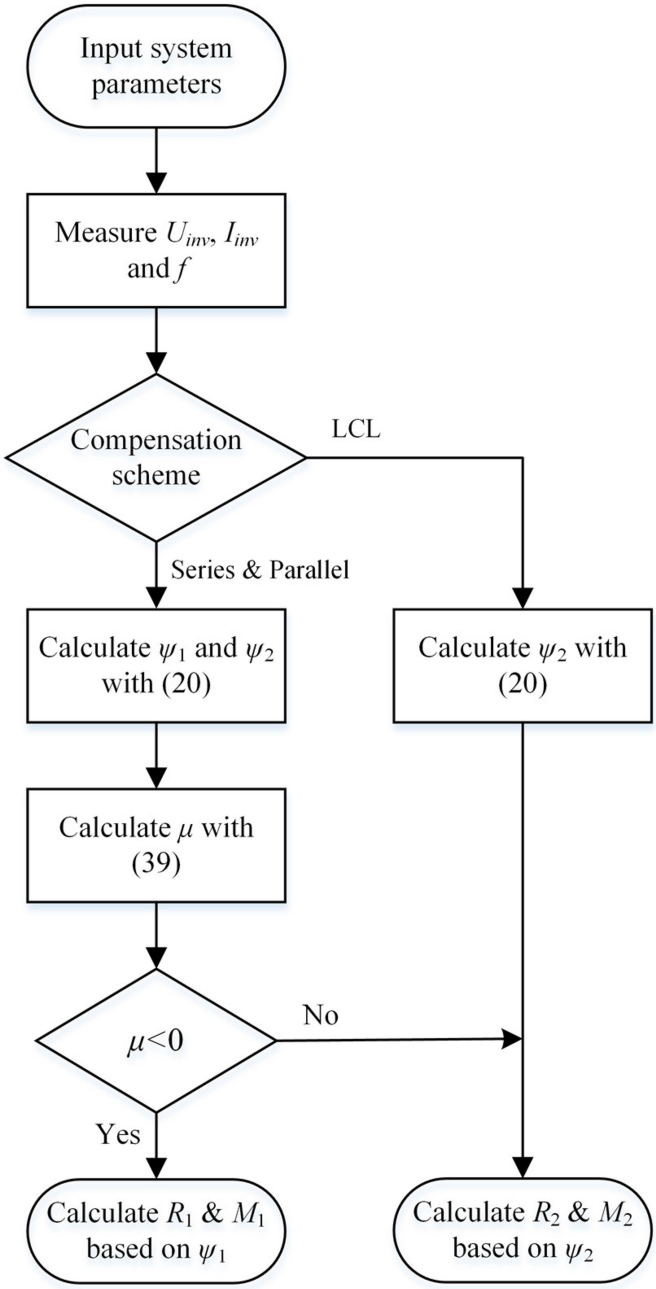

Fig. 8. Flowchart of the proposed identification method.

frequency. Under this condition, several expressions proposed in this section will be different, which are discussed in the following.

When the system operates at the other frequency instead of ZPA frequency, there will be a phase difference ϕ between $u_{\rm inv}$ and $i_{\rm inv}$, and the input impedance $Z_{\rm in}$ should be

$$Z_{\rm in} = \frac{\dot{U}_{\rm inv}}{\dot{I}_{\rm inv}} = \frac{U_{\rm inv}}{I_{\rm inv}} \left(\cos\phi - j\sin\phi\right). \tag{40}$$

TABLE III
PARAMETERS OF THE IPT SYSTEMS

	S/P & P/P	LCL/P
L_p/μH	152.87	152.87
C_p/nF	68.26	138.61
R_p/Ω	0.49	0.49
L_s/μH	153.60	153.60
C_s/nF	67.73	67.73
R_s/Ω	0.54	0.54
L_r/μH	–	156.02
R_r/Ω	–	2.9

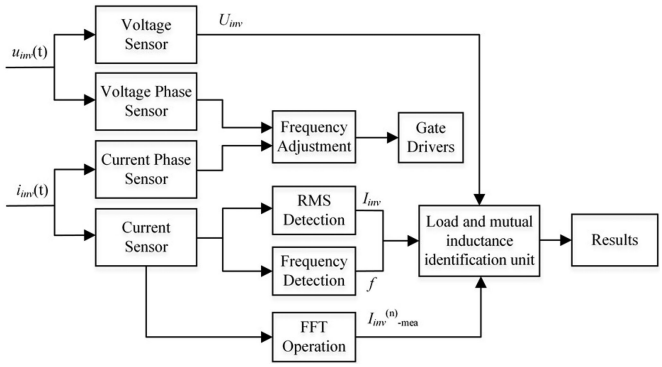

Fig. 9. Structure of the proposed identification method.

Furthermore, (8), (9), and (11) will be expressed as (41)–(43), respectively,

$$\Re\left(Z_{\rm in}\right) = \frac{U_{\rm inv}}{I_{\rm inv}} \cdot \cos\phi \tag{41}$$

$$\Im\left(Z_{\rm in}\right) = \frac{U_{\rm inv}}{I_{\rm inv}} \cdot \sin\phi \tag{42}$$

$$Z_\theta = \frac{1}{Z_{11} - Z_{\rm in}} = \frac{Z_{22}}{Z_{12}^2}. \tag{43}$$

The value of Z_θ can still be calculated by measuring $u_{\rm inv}$, $i_{\rm inv}$, f and ϕ. The rest of calculation procedure shown in (12)-(22) will be same. The way to eliminate the undesired solution is similar to the case when the system operates at ZPA frequency (i.e., the negative solution or the solution which leads to a larger $\sigma(n)_{-i}$ will be eliminated).

IV. Simulation and Experiment Verification

In order to verify the effectiveness of the proposed method, a simulation model based on MATLAB/Simulink is set up with reference to Fig. 1. The total simulation time is set at 1 ms and the system has already reached the steady state. The maximum simulation step is 0.1 μs. The main parameters are the same in both simulation and experiment systems, and they are listed in Table III.

The structure diagram of the proposed identification method is shown in Fig. 9. The zero phase angle condition is achieved by the frequency adjustment. The values of $U_{\rm inv}$, $I_{\rm inv}$ and f are measured by the detection units; $I^{(3)}_{\rm inv\_mea}$ and $I^{(5)}_{\rm inv\_mea}$ can be obtained by the fast Fourier transformation (FFT) operation.

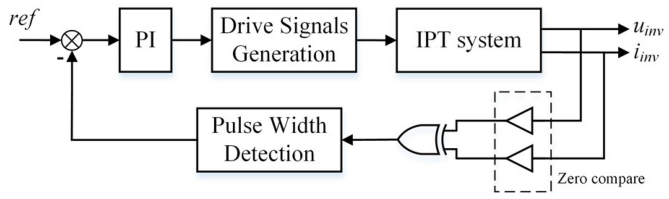

Fig. 10. Frequency control block.

Then, the algorithm is conducted in load and mutual inductance identification unit by the measured values.

In the frequency adjustment module, the output signals of the voltage and current sensors are compared with zero, then two square waves can be detected. Based on the exclusive or (XOR) operation between these two square waves, a pulse square wave, whose pulse width represents the phase difference between the voltage and current, could be achieved. A larger phase difference results in a larger pulse width of the square wave. Thus, the pulse width can be minimized by regulating the frequency of the drive signal to keep the input voltage and current in phase. The control strategy of the ZPA frequency is shown in Fig. 10.

A. Simulation Results

Simulation studies were carried out when the mutual inductance changes from 15 to 45 μH, while the load resistance changes from 20 to 60 Ω. Only partial calculated results and measured values are listed in Table IV due to the large amount of data. It can be seen that, for the primary LCL compensation, the calculation of M_1 and μ is unnecessary because ψ_1 is negative (R_1 and ψ_1 have the same sign), then R_1 and M_1 should be eliminated. For the primary series and parallel compensation, R_2 and M_2 are considered as the actual identification results due to the positive μ. These results are coincident with the above theoretical analysis.

The entire load and mutual inductance identification results are shown in Fig. 11. All the identification results of the equivalent load resistance and mutual inductance are in good agreement with the set values, and the maximum identification error of all the simulation results is less than 3%. The main causes of the identification error in the simulation are listed as follows.

1) In the circuit model, only the fundamental harmonic is taken into consideration and the higher harmonics are neglected. Therefore, this approximate circuit model will bring a small identification error.
2) The simulation model was carried out discretely in MATLAB, which will bring in error. The identification algorithm are realized based on the results of the simulation model, which finally results in the identification error.

B. Experimental Results

A practical IPT experimental setup with the parameters shown in Table III has been built and practically tested. The FFT operation and the identification model were implemented on the field–programmable gate array (FPGA) (Altera Cyclone II EP2C5T144C8), and the full-bridge inverter circuit is made up of four MOSFETs (STP30NF20). The output of the voltage and

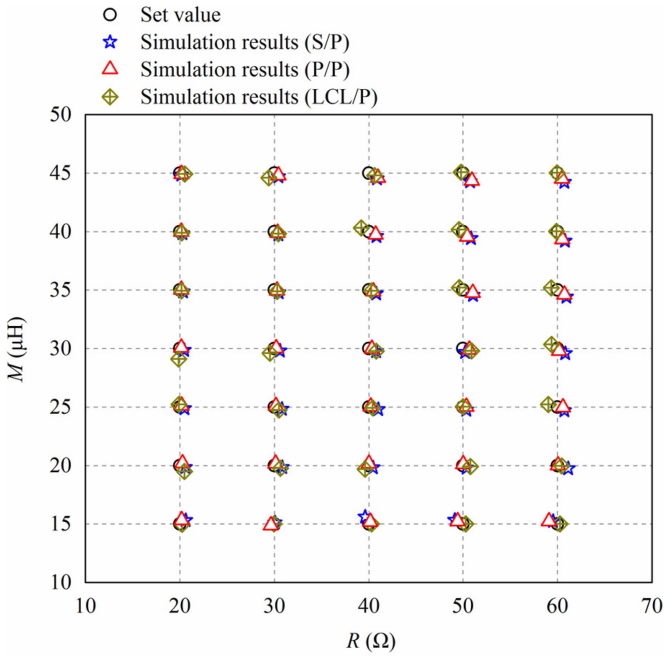

Fig. 11. Identification simulation results.

current sensors were connected up to the high-speed ADC chip (AD9226). In each sampling period, the discrete values of the voltage and current were measured and transferred to the FPGA chip. Then, the RMS value can be calculated by the FPGA based on these discrete data. Furthermore, the time between two adjacent zero-crossing points of the current can be obtained according to the discrete current values, based on which the operating frequency can be calculated.

The experimental setup of series-parallel compensated IPT system is illustrated in Fig. 12(a). The load is made up of several resistors shown in Fig. 12(b) and the resistance can be changed by pressing the buttons. The mutual inductance can be changed by adjusting the relative position between the transmitting coil and the receiving coil. In addition, it should be noted that the primary compensation presented in Fig. 12(a) is series-compensation, and this module will be different if the primary-resonant tank is changed to the parallel compensation or the LCL compensation.

When the load resistance is fixed at 30 Ω and the mutual inductance is changed from 15 to 45 μH (the measured values are 15.06, 19.87, 24.86, 30.56, 35.75, 39.78, and 45.78 μH, respectively), the identification method was implemented and the results shown in Fig. 13 were obtained.

Similarly, the experiments with the fixed mutual inductance and the different load resistances have been completed. The mutual inductance is fixed at 31.02 μH and the load resistance is changed from 20 to 60 Ω. Then, the identification results are illustrated in Fig. 14.

The maximum identification errors are given in Table V and the identification results have errors less than 7%. In this paper, the conduction loss and radiation loss have been ignored. Besides, there are always some measurement errors in the actual system. Consequently, the identification accuracy of the exper-

TABLE IV
PART OF SIMULATION DATA

	R_{set}/Ω	M_{set}/μH	R_1/Ω	M_1/μH	R_2/Ω	M_2/μH	μ	U_{mea}/V	I_{mea}/A	f/kHz
S/P	30	30	4015.2	6.62	30.63	29.81	7.7×10^{-3}	20.0	10.88	50.23
	40	30	2429.9	7.33	40.82	29.75	2.1×10^{-3}	20.0	8.88	50.23
	50	30	1762.2	8.17	50.24	29.67	3.5×10^{-3}	20.0	7.62	50.24
P/P	30	30	4306.7	6.58	30.20	30.03	1.7×10^{-3}	22.2	18.96×10^{-3}	50.21
	40	30	2643.3	7.20	40.36	29.97	2.1×10^{-3}	22.2	23.27×10^{-3}	50.20
	50	30	1926.4	7.92	50.67	29.89	1.5×10^{-3}	22.2	27.56×10^{-3}	50.19
LCL/P	30	30	−2700.9	–	29.55	29.60	–	20.0	3.79	49.09
	40	30	−2332.0	–	40.83	29.77	–	20.0	3.48	49.07
	50	30	−2005.7	–	50.91	29.81	–	20.0	3.22	49.05

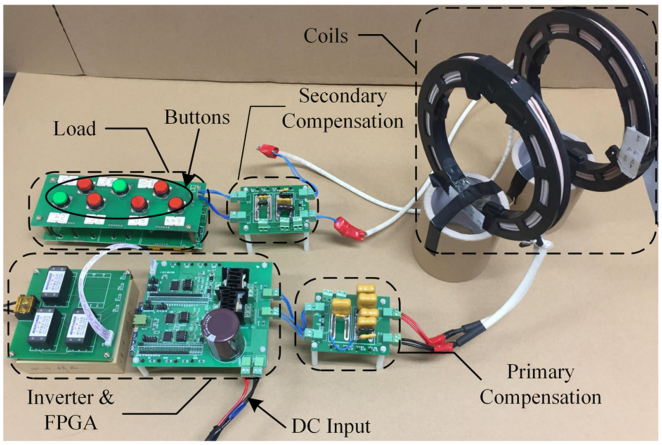

Fig. 12. Experimental setup. (a) Prototype. (b) Bottom view of load.

TABLE V
MAXIMUM ERROR OF EXPERIMENTAL RESULTS

Maximum error		S/P	P/P	LCL/P
Fixed R	δ_R	3.37%	4.07%	5.60%
	δ_M	4.63%	6.68%	4.05%
Fixed M	δ_R	4.02%	5.10%	3.80%
	δ_M	6.35%	5.25%	4.51%

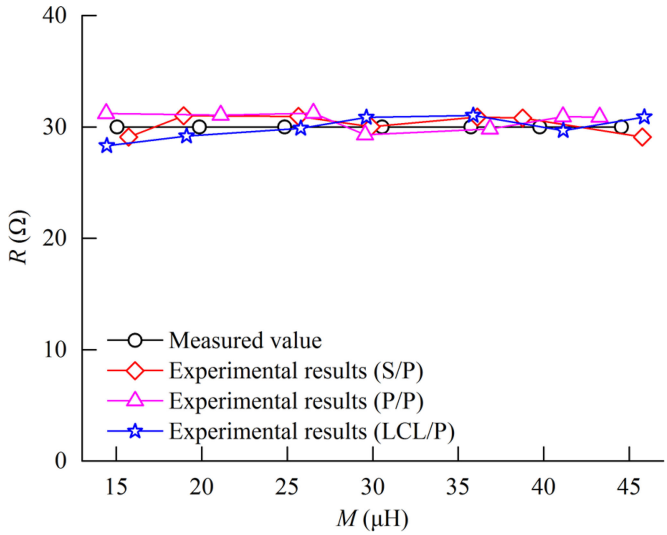

Fig. 13. Identification results when the load resistance is fixed.

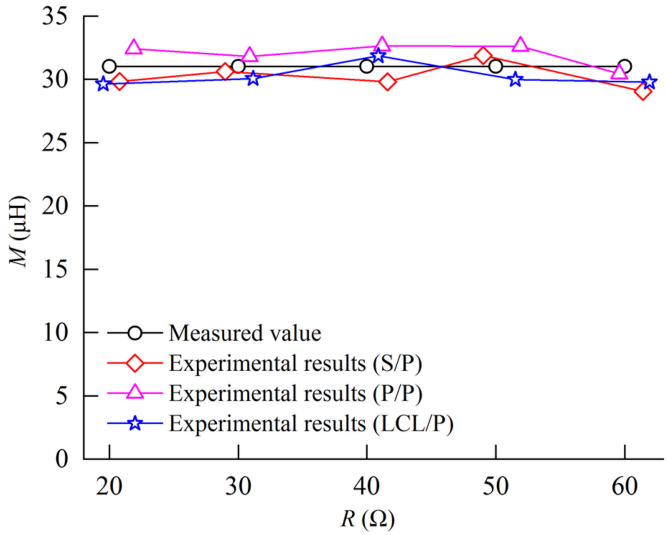

Fig. 14. Identification results when the mutual inductance is fixed.

imental results are lower than the simulation results. Overall, these experimental results verified the feasibility and accuracy of the proposed identification method.

V. CONCLUSION

This paper has proposed a load and mutual inductance identification method for IPT systems with parallel compensation at the secondary side. The proposal has been implemented for

series, parallel, and LCL compensations, which are commonly used tuning schemes employed in the primary side of IPT systems. The load resistance and mutual inductance have been identified by detecting the system operating frequency, the output voltage and current of the inverter. It has found the simulation results and the set values are in close agreements, and the maximum identification errors of the experimental results are less than 7%. Both the simulation and experimental results have verified the feasibility of the proposed load and mutual inductance identification method.

REFERENCES

[1] G. A. Covic and J. T. Boys, "Inductive power transfer," *Proc. IEEE*, vol. 101, no. 6, pp. 1276–1289, Jun. 2013.

[2] W. Zhang and C. C. Mi, "Compensation topologies of high-power wireless power transfer systems," *IEEE Trans. Veh. Technol.*, vol. 65, no. 6, pp. 4768–4778, Jun. 2016.

[3] J. Tian and A. P. Hu, "A DC-voltage-controlled variable capacitor for stabilizing the ZVS frequency of a resonant converter for wireless power transfer," *IEEE Trans. Power Electron.*, vol. 32, no. 3, pp. 2312–2318, Mar. 2017.

[4] J. H. Kim *et al.*, "Development of 1-MW inductive power transfer system for a high-speed train," *IEEE Trans. Ind. Electron.*, vol. 62, no. 10, pp. 6242–6250, Oct. 2015.

[5] S. Y. Choi, B. W. Gu, S. Y. Jeong, and C. T. Rim, "Advances in wireless power transfer systems for roadway-powered electric vehicles," *IEEE Trans. Emerging Sel. Topics Power Electron.*, vol. 3, pp. 18–36, Mar. 2015.

[6] D. H. Tran, V. B. Vu, and W. Choi, "Design of a high-efficiency wireless power transfer system with intermediate coils for the on-board chargers of electric vehicles," *IEEE Trans. Power Electron.*, vol. 33, no. 1, pp. 175–187, Jan. 2018.

[7] J. E. I. James, A. Chu, D. Robertson, A. Sabitov, and G. A. Covic, "A series tuned high power IPT stage lighting controller," in *Proc. Energy Convers. Congr. Expo.*, 2011, pp. 2843–2849.

[8] D. Robertson, A. Chu, A. Sabitov, and G. A. Covic, "High power IPT stage lighting controller," in *Proc. Int. Symp. Ind. Electron.*, 2011, pp. 1974–1979.

[9] S. Y. Hui and W. Ho, "A new generation of universal contactless battery charging platform for portable consumer electronic equipment," *IEEE Trans. Power Electron.*, vol. 20, no. 3, pp. 620–627, May 2005.

[10] S. Y. Hui, "Planar wireless charging technology for portable electronic products and qi," *Proc. IEEE*, vol. 101, no. 6, pp. 1290–1301, Mar. 2013.

[11] A. P Hu, Y. W. You, F. B. Chen, D. McCormick, and D. M. Budgett, "Wireless power supply for ICP devices with hybrid supercapacitor and battery storage," *IEEE J. Emerging Sel. Topics Power Electron.*, vol. 4, no. 1, pp. 273–279, Mar. 2016.

[12] M. R. Basar, M. Y. Ahmad, J. cho, and F. Ibrahim, "Stable and high-efficiency wireless power transfer system for robotic capsule using a modified Helmholtz coil," *IEEE Tran. Ind. Electron.*, vol. 64, no. 2, pp. 1113–1122, Feb. 2017.

[13] W. Zhang, S. Wong, C. K. Tse, and Q. Chen, "Load-independent duality of current and voltage outputs of a series- or parallel-compensated inductive power transfer converter with optimized efficiency," *IEEE J. Emerging Sel. Topics Power Electron.*, vol. 3, no. 1, pp. 137–146, Mar. 2015.

[14] W. X. Zhong and S. Y. R. Hui, "Maximum energy efficiency tracking for wireless power transfer systems," *IEEE Trans. Power Electron.*, vol. 30, no. 7, pp. 4025–4034, Jul. 2015.

[15] D. Seo, J. Lee and H. Lee, "Optimal coupling to achieve maximum output power in a WPT system," *IEEE Trans. Power Electron.*, vol. 31, no. 6, pp. 3994–3998, Jun. 2016.

[16] J. M. Miller, O. C. Onar, and M. Chinthavali, "Primary-side power flow control of wireless power transfer for electric vehicle charging," *IEEE J. Emerging Sel. Topics Power Electron.*, vol. 3, no. 1, pp. 147–162, Mar. 2015.

[17] M. Fu, H. Yin, X. Zhu, and C. Ma, "Analysis and tracking of optimal load in wireless power transfer systems," *IEEE Trans. Power Electron.*, vol. 30, no. 7, pp. 3952–3963, Jul. 2015.

[18] T. Yeo, D. Kwon, S. Khang, and J. Yu, "Design of maximum efficiency tracking control scheme for closed-loop wireless power charging system employing series resonant tank," *IEEE Trans. Power Electron.*, vol. 32, no. 1, pp. 471–478, Jan. 2017.

[19] Z. Wang, Y. Li, Y. Sun, C. Tang, and X. Lv, "Load detection model of voltage-fed inductive power transfer system," *IEEE Trans Power Electron.*, vol. 28, no. 11, pp. 5233–5243, Feb. 2013.

[20] J. Yin, D. Lin, C. Lee, and S. Y. R. Hui, "A systematic approach for load monitoring and power control in wireless power transfer systems without any direct output measurement," *IEEE Trans. Power Electron.*, vol. 30, no. 3, pp. 1657–1667, Apr. 2015.

[21] Y. Su, L. Chen, Z. Wang, A. P. Hu, and X. Dai, "A load identification method for inductive power transfer system based on the least squares algorithm," *Trans. China Electrotech. Soc.*, vol. 30, pp. 9–14, Mar. 2015.

[22] J. Yin, D. Lin, C. K. Lee, T. Parisini, and S. Y. R. Hui, "Front-end monitoring of multiple loads in wireless power transfer systems without wireless communication systems," *IEEE Trans. Power Electron.*, vol. 31, no. 3, pp. 2510–2517, Mar. 2016.

[23] Y. Su, H. Zhang, Z. Wang, A. P. Hu, L. Chen, and Y. Sun, "Steady-state load identification method of inductive power transfer system based on switching capacitors," *IEEE Trans. Power Electron.*, vol. 30, no. 11, pp. 6349–6355, Nov. 2015.

[24] J. Yin, D. Lin, T. Parisini, and S. Y. R. Hui, "Front-end monitoring of the mutual inductance and load resistance in a series-series compensated wireless power transfer system," *IEEE Trans. Power Electron.*, vol. 31, no. 10, pp. 7339–7352, Oct. 2016.

[25] D. Ahn and S. Hong, "Wireless power transmission with self-regulated output voltage for biomedical implant," *IEEE Trans. Ind. Electron.*, vol. 61, no. 5, pp. 2225–2235, May 2014.

[26] Z. Pantic and S. M. Lukic, "Framework and topology for active tuning of parallel compensated receivers in power transfer systems," *IEEE Trans. Power Electron.*, vol. 27, no. 11, pp. 4503–4513, Nov. 2012.

[27] C. Wang, G. A. Covic and O. H. Stielau, "Power transfer capability and bifurcation phenomena of loosely coupled inductive power transfer systems," *IEEE Trans. Ind. Electron.*, vol. 51, no. 1, pp. 148–157, Feb. 2004.

[28] M. J. Neath, A. K. Swain, U. K. Madawala, and D. J. Thrimawithana, "An optimal PID controller for a bidirectional inductive power transfer system using multiobjective genetic algorithm," *IEEE Trans. Power Electron.*, vol. 29, no. 3, pp. 1523–1531, Mar. 2014.

Yu-Gang Su (M'09) received the B.E. and M.E. degrees in industry automation and the Ph.D. degree in control theory and control engineering from Chongqing University, Chongqing, China, in 1985, 1993, and 2004, respectively.

From 2008 to 2009, he was a Visiting Scholar with the University of Queensland, Brisbane, QLD, Australia. He is currently a Professor with the College of Automation, Chongqing University. His research interests include power electronics, control theory and applications, and wireless power transfer.

Long Chen received the B.S. degree in medical information from Southern Medical University, Guangzhou, China, in 2011. He is currently working toward the Ph.D. degree in control theory and control engineering at the College of Automation, Chongqing University, Chongqing, China.

His current research interests include the load identification and optimization of wireless power transfer systems.

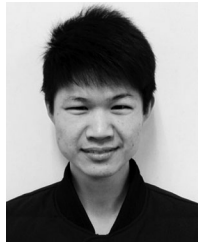

Xue-Ying Wu received the B.E. degree in electronic information science and technology from the College of Physics and Electronic Engineering, Yangtze Normal University, Chongqing, China, in 2014. He is currently working toward the Ph.D. degree in control theory and control engineering from the College of Automation, Chongqing University, Chongqing, China.

His current research interests include wireless power transfer technologies, parameters optimization of capacitively coupled power transfer systems and its control strategy.

Aiguo Patrick Hu (M'01–SM'07) received the Graduate degree electical engineering from Xian JiaoTong University, Xian, China and the B.E. and M.E. degrees in 1985 and 1988, respectively. He received the Ph.D. degree in electical engineering from the University of Auckland, Auckland, New Zealand, in 2001.

He was a Lecturer, the Director of the China Italy Cooperative Technical Training Center, Xian, China, and the General Manager of a technical development company. Funded by the Asian2000 Foundation, he stayed in the National University of Singapore for a semester as an exchange Postdoc Research Fellow. He holds 15 patents in wireless/contactless power transfer and microcomputer control technologies, has published more than 200 peer reviewed journal and conference papers, authored a monograph on wireless inductive power transfer technology, and contributed 4 book chapters. He is currently with the Department of Electrical and Computer Engineering, University of Auckland, and also the Head of Research of PowerbyProxi Ltd. His research interests include wireless/contactless power transfer systems and application of power electronics in renewable energy systems.

Chun-Sen Tang (S'08–M'09) received the B.E. and Ph.D. degrees from the College of Automation, Chongqing University, Chongqing, China, in 2004 and 2009, respectively.

In 2008, he was a Research Fellow with the Department of Electrical and Computer Engineering, University of Auckland, Auckland, New Zealand. In 2009, he joined College of Automation, Chongqing University, Chongqing, China, where he is currently an Associate Professor. His current research interests include nonlinear modeling and analysis, intelligent control, and wireless power transfer.

Xin Dai (M'10) received the B.E. degree in industrial automation from Yuzhou University, Chongqing, China, in 2000 and the Ph.D. degree in control theory and control engineering from the College of Automation, Chongqing University, Chongqing, in 2006.

In 2012, he was a Visiting Scholar with the University of Auckland, Auckland, New Zealand. He is currently a Professor with the College of Automation, Chongqing University. His current research interests include inductive power transfer technology and nonlinear dynamic behavior analysis of power electronics.